

2 Remote Sensing Change Detection in Urban Environments

John R. Jensen, Department of Geography, University of South Carolina, Columbia, SC

Jungho Im, Department of Geography, University of South Carolina, Columbia, SC

2.1 Introduction

Timely and accurate change information in the urban environment is essential for successful planning and management. The change detection may range from 1) monitoring general land cover/land use found in multiple dates of imagery, to 2) anomaly (e.g., subsidence) detection on hazardous waste sites. Remote sensing approaches to change detection have been widely used due to its cost-effectiveness, extensibility, and temporal frequency. Since the advent of high-spatial resolution satellite imagery, it has become increasingly popular to detect, analyze, and monitor detailed changes such as new buildings, roads, and even patios in the urban environment. Basically, there are two types of change detection methods: 1) detection of the change using various image enhancement methods, and 2) extraction of detailed types of land-cover change based on the use of classification techniques (Chan et al. 2001; Jensen 2005)

Traditional remote sensing change detection techniques, which are generally applicable to coarse spatial resolution optical imagery, include image algebra multi-band differencing (Coppin and Bauer 1996), image transformation such as principal components analysis (Collins and Woodcock 1996), and the widely used post-classification comparison method (Jensen et al. 1995). More recent change detection methods are based on expert

systems, artificial neural networks, fuzzy sets, and object-oriented approaches. These change detection methods are explained in Lu et al. (2004) and Jensen (2005).

This chapter provides several examples of remote sensing change detection based on new change detection techniques using the remote sensor data obtained from 1) a digital frame camera, and 2) a LIDAR (Light Detection and Ranging) sensor system. These sensors function according to the logic shown in Figure 1. The change detection techniques include neighborhood correlation image analysis and single date elevation-based subsidence detection.

2.2 Remote Sensing Change Detection Process

Jensen (2005) reviews the general steps that are used to conduct change detection using remotely sensed data. The steps include 1) specifying the nature of the change detection problem, 2) identifying the remote sensing system and environmental considerations associated with change detection, 3) processing remote sensor data to extract change information by applying appropriate change detection techniques, and 4) evaluating the change detection results. Using these steps, scientists are able to decide whether their change detection results are of value. Selecting appropriate remote sensor data and change detection techniques according to the nature of the change detection problem under investigation is critical in change detection studies.

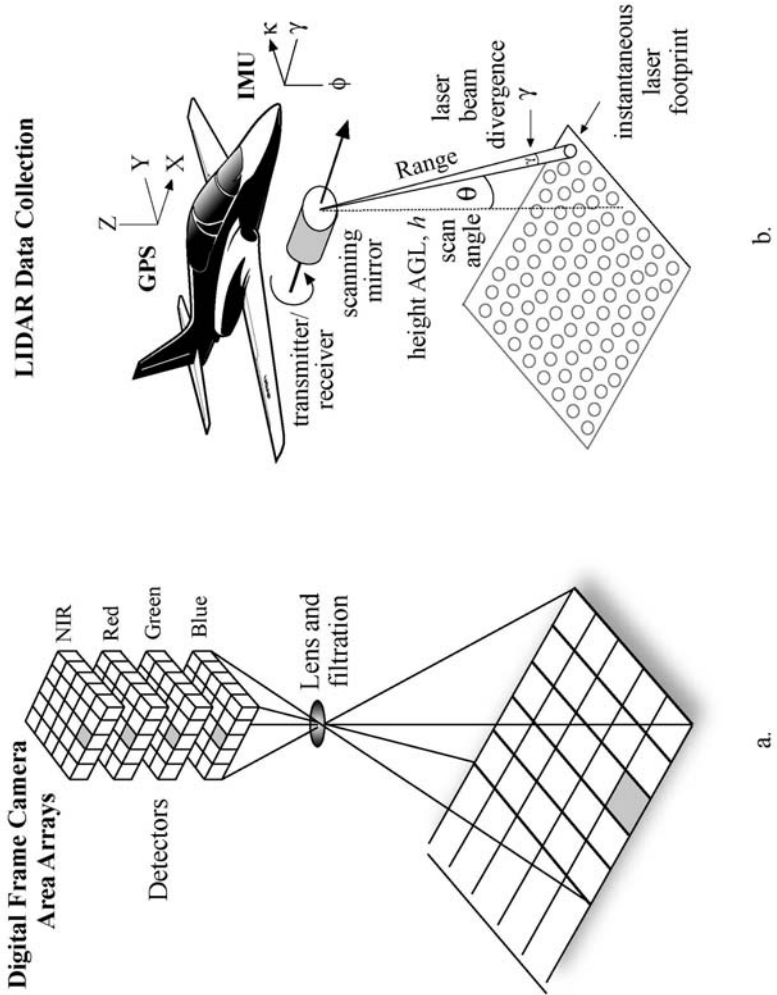


Fig. 1. Two remote sensor systems often used to collect information in the urban environment. a) Digital frame camera based on area arrays. b) LIDAR scanner.

2.2.1 Digital Frame Camera Remote Sensing

Digital frame cameras have many similarities to regular cameras. Instead of film, however, they use an area array of charge-couple-devices (CCD) detectors (Figure 1). Like a traditional camera system, the digital CCD area array records a “frame” of terrain during a single exposure. Three parameters determine the geographic area of the terrain recorded by the CCD area array, including 1) the dimension of the CCD array in rows and columns, 2) the focal length of the camera lens (the distance from the rear nodal point of the lens to the CCD array), and 3) the altitude of the aircraft above ground level (Jensen 2005). A major advantage of digital frame camera remote sensing is its timeliness. The remote sensor data are available as soon as they are collected since there is no need for an analog-to-digital (A to D) conversion.

2.2.2 LIDAR Remote Sensing

LIDAR is an optical remote sensing system that uses near-infrared laser light to measure the range from the sensor to a target on the surface of the Earth. Three fundamental technologies are used in the LIDAR system, including 1) laser range-finding, 2) differential global positioning system (DGPS), and 3) inertial measurement units (IMUs). LIDAR was initially introduced to facilitate the data collection for digital elevation models (DEM). Digital elevation information is a critical component of most geographic databases used by many agencies such as the USGS and FEMA. Digital elevation models can be subdivided into digital surface models (DSM) and digital terrain models (DTM). DSM contain elevation information about all features in the landscape, including vegetation and buildings. DTM contain elevation information solely about the bare-Earth surface (Jensen 2006). LIDAR technology can be used to generate the two types of elevation models.

Most LIDAR systems that are used for terrestrial topographic mapping use near-infrared light from 1040 to 1060 nm. Blue-green laser light centered at approximately 532 nm is used for bathymetric mapping due to its water penetration capability (Mikhail et al. 2001; Boland et al. 2004). Since LIDAR is an active system, it can also be used at night. The accurate measurement of the laser pulse travel time from a light transmitter to a target on the ground and back to a receiver is critical in the LIDAR systems. The range measurement process produces elevation data points, which are commonly referred to as masspoints.

One of the advantages of LIDAR remote sensing is that each LIDAR point is already georeferenced. It does not require additional geometric correction (Flood and Gutelius 1997). LIDAR systems receive multiple returns depending on the type of a target on the Earth surface. If a laser pulse hits directly on the ground, it will be recorded as a single return. If there are any materials (trees, grass) with local relief within the instantaneous footprint of a pulse, then the pulse will produce multiple returns (first, second ... last returns). First returns including single returns can be used to generate a DSM, while last returns can be used to create a DTM. Additional processing is generally required to generate a DTM from last returns because some laser pulses never make it to the ground in heavily forested areas.

Most LIDAR systems provide intensity information in addition to the multiple return range data. The recorded intensity is in most cases just the maximum of the returned signals (Baltasvias 1999). The intensity values are dependent on several factors including gain setting, bidirectional effects, the size of the target, range to the target, angle of incidence and atmospheric dispersion (Leonard, 2005).

Neighborhood Correlation Image Analysis

The Neighborhood Correlation Image (NCI) analysis concept was introduced by Im and Jensen (2005). Correlation analysis can be applied to bi-temporal imagery in a specified neighborhood to extract spectral *contextual* information, which contains three unique variables associated with the change in two dates of imagery. These variables include neighborhood correlation, neighborhood slope, and neighborhood intercept. The neighborhood correlation variable represents Pearson's product-moment correlation coefficient between the brightness values from bi-temporal imagery in a specified neighborhood. The neighborhood slope and intercept variables are calculated using the least squares estimates from the sets of brightness values:

$$correlation = \frac{\sum_{i=1}^n \sum_{j=1}^k (BV_{ij1} - \mu_1)(BV_{ij2} - \mu_2)}{s_1 s_2 (n \times k - 1)} \quad (1)$$

$$\text{slope} = \frac{\sum_{i=1}^n \sum_{j=1}^k (BV_{ij1} - \mu_1)(BV_{ij2} - \mu_2)}{s_1^2 (n \times k - 1)} \quad (2)$$

$$\text{intercept} = \frac{\sum_{i=1}^n \sum_{j=1}^k BV_{ij2} - a \sum_{i=1}^n \sum_{j=1}^k BV_{ij1}}{n \times k} \quad (3)$$

where n is the number of pixels in a specified neighborhood, and k is the number of bands in each dataset. s_1 and s_2 are the standard deviations of the brightness values found in all bands of each dataset in a specified neighborhood, respectively. BV_{ij1} and BV_{ij2} are the i th brightness values of the pixels found in band k of the Date 1 and Date 2 images in a specified neighborhood, and μ_1 and μ_2 are the means of brightness values found in all bands of the Date 1 and Date 2 images in a specified neighborhood, respectively.

If the spectral changes of the pixels within a specified neighborhood between the two dates are significant, the correlation coefficient between the two sets of brightness values in the neighborhood will decrease to a lower value. The slope and intercept values may increase or decrease depending on the magnitude and direction of the spectral changes. Ideally, if there is no change in a certain pixel location between two dates, the pixel will have high correlation, a slope around 1, and an intercept around 0. An example of correlation analysis with two sample locations (change vs. no change) from bi-temporal ADAR digital frame camera imagery is shown in Figure 2.

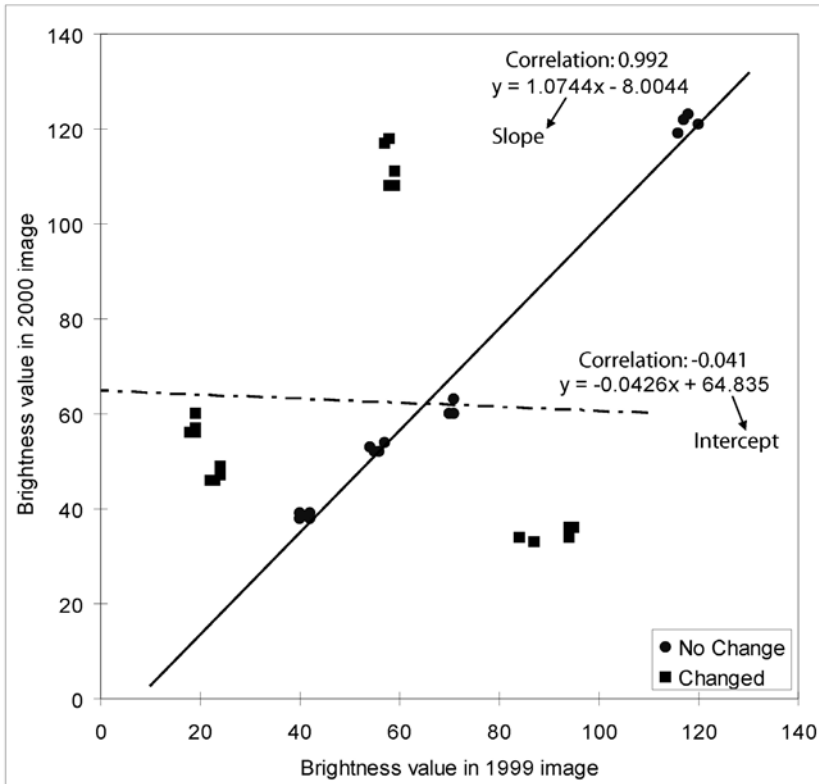


Fig. 2. An example of correlation analysis with two sample locations (change versus no change) based on the analysis of bi-temporal ADAR imagery.

Several shapes of neighborhood can be applied to neighborhood correlation image analysis within a GIS context, including rectangle, circle, annulus, wedge, and irregular. A module to create NCIs was developed as a dynamic linked library (DLL) in the ESRI ArcMap 9.1 environment using Visual Basic. Two general shapes – rectangle (square) and circle – of neighborhood were incorporated into the module. The size of neighborhood can be specified by users (e.g., 3×3).

2.3 Case Study 1 – Land Cover Change Detection Using NCI Analysis and Decision Tree Classification

The objectives of this study were to explore three types of neighborhood correlation image variables using several neighborhood configurations and to extract detailed “from-to” change information from bi-temporal imagery plus the NCIs using a decision tree classifier (Im and Jensen 2005). This study examined five different sizes of circular neighborhoods (i.e., 1- to 5-pixel radius). The study area, located in Edisto Beach near Charleston, SC, exhibited considerable residential development between two dates of imagery. The processing steps required to implement the change detection study based on neighborhood correlation image analysis and decision tree classification are summarized in Figure 3.

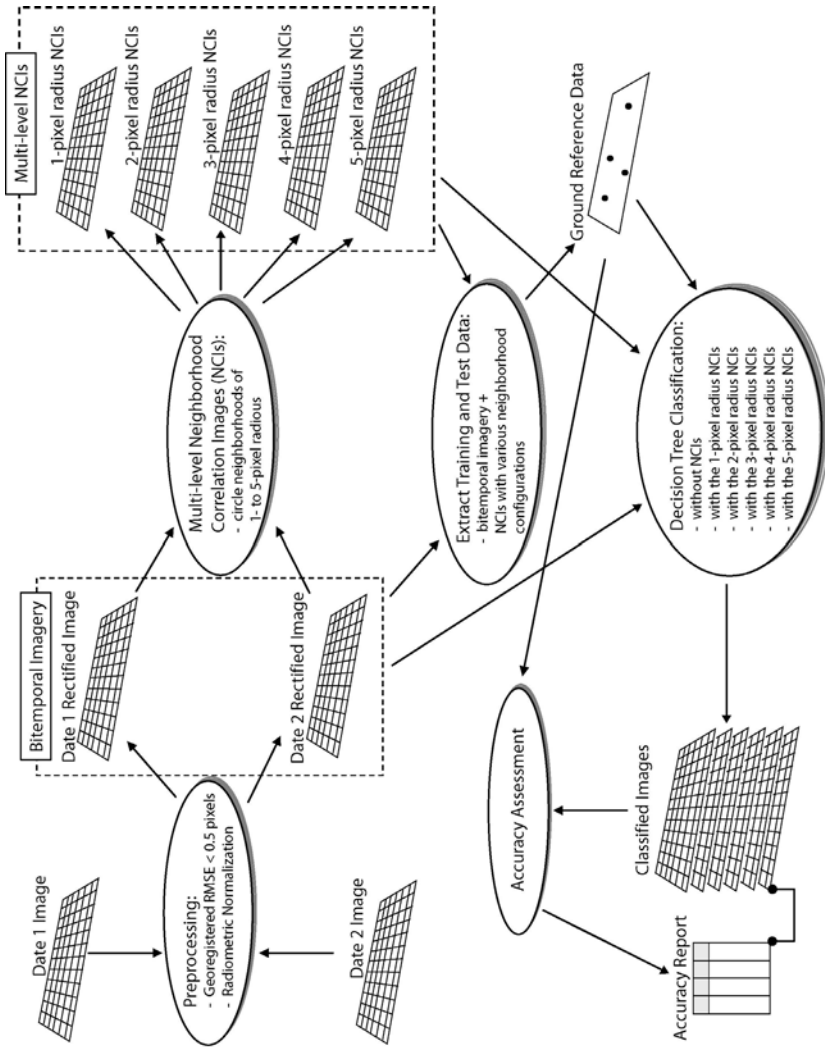


Fig. 3. Data processing flow diagram of the urban case study.

Bi-temporal remote sensing data were collected on September 23, 1999 and October 10, 2000 over the study area using an ADAR 5500 area array frame camera in four spectral bands, which included the blue, green, red, and near-infrared (Figure 4a,b). The multispectral data were preprocessed

(coregistered and radiometrically normalized) before the creation of neighborhood correlation images and subsequent change detection.

Eight hundred checkpoints were randomly generated and used as ground reference information. Each checkpoint was investigated using visual interpretation and assigned to one of thirteen land cover change classes. The classes included eight change classes (Barren to Developed, Tree to Developed, Tree to Barren, Grass to Barren, Barren to Grass, Tree to Grass, Tree to Shadow, and Change in Grass) and five unchanged classes (Developed, Barren, Tree, Grass, and Shadow). Five hundred of the samples were used to train a decision tree classifier. The remaining three hundred samples were used to evaluate the accuracy of the change classification.

Five sizes of circle neighborhoods were explored (1- to 5-pixel radius). Figures 4c-e depict the 1-pixel radius neighborhood correlation image variables. Based on visual inspection, large neighborhood sizes (e.g., 5-pixel radius) reduced noise e.g., caused by shadow difference in the NCIs, yielding a smoothing effect in the images. However, it altered change information (size) to some extent, e.g., a narrow linear change was barely distinguishable in the NCIs. Conversely, the use of a small neighborhood size helps detect change more precisely, but can introduce some noise. Two-dimensional planes between the 3-pixel neighborhood correlation image variables based on the eight hundred reference data are shown in Figure 5. In most cases, the unchanged samples resulted in high correlation values and slope values ~ 1 and intercept values ~ 0 . Conversely, the changed samples generally exhibited low correlation values and variant slope and intercept values. Although a few changed samples yielded relatively high correlation (e.g., Barren to Developed), they were distinguishable using the other two variables (i.e., slope and intercept). These three unique change variables were very useful for the identification of change versus no change in the study area.

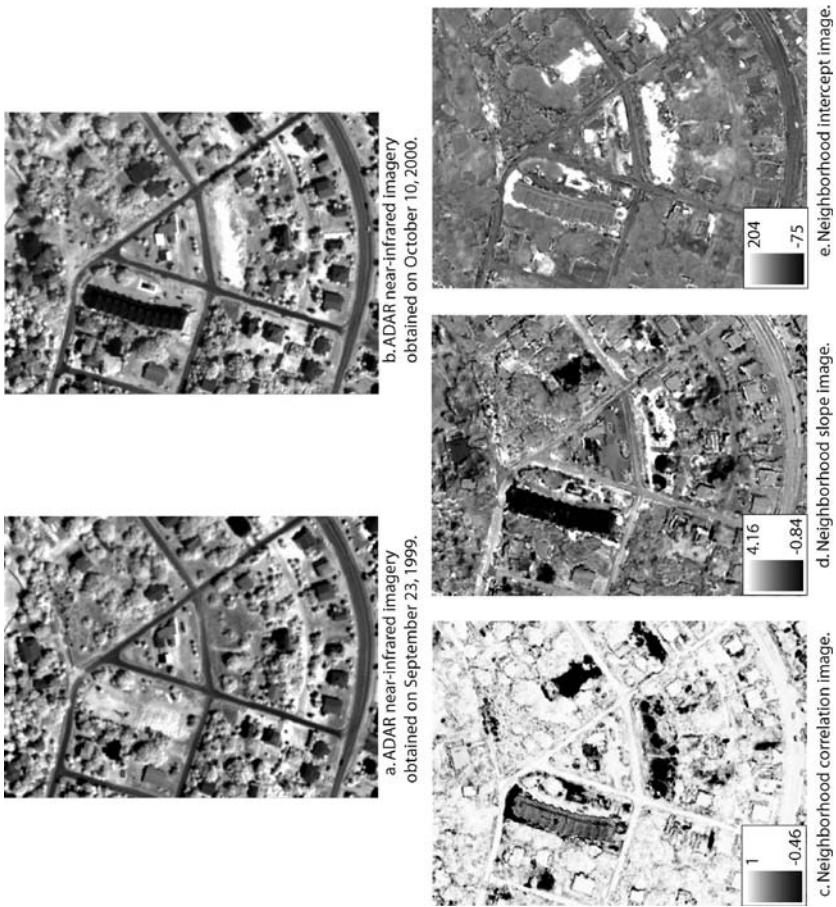


Fig. 4. a), b) Bi-temporal ADAR near-infrared imagery obtained on September 23, 1999 and on October 10, respectively. c) - e) Neighborhood correlation images (correlation, slope, and intercept) created from the bi-temporal ADAR imagery.

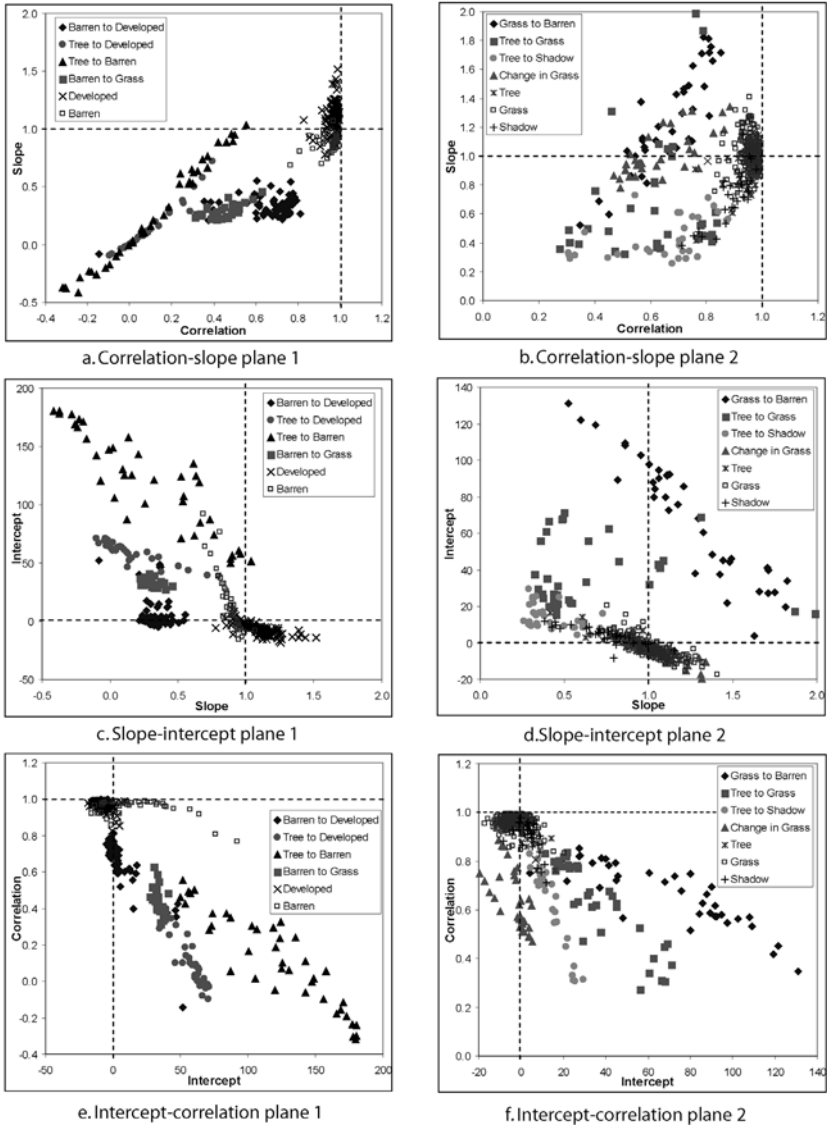


Fig. 5. Two-dimensional planes between the three NCI variables using the reference data.

The C5.0 decision tree was utilized to classify the land cover change using the bi-temporal data plus the NCI information. A detail discussion of C5.0 is found in Jensen (2005) and Quinlan (2003). Five hundred samples were

used to train a decision tree classifier and the remaining three hundred samples were used to evaluate the change classification. In order to apply the decision tree generated from C5.0 to the corresponding imagery, a C5.0 decision tree inference engine was developed and embedded in the ESRI ArcMap 9.1. All change classifications that included the NCIs resulted in significantly higher Kappa accuracies than the change classification based solely on the use of bi-temporal imagery (Table 1a). The change classification that incorporated the 3-pixel neighborhood correlation images produced the highest accuracy (overall accuracy = 94.3%; Kappa = 0.94). Figure 6 shows the change classification output image using the 3-pixel radius NCIs and the change detection matrix between the two dates.

Table 1. a) Land-cover change classification results based on the thirteen classes using a decision tree classifier.

Category	Overall accuracy	Kappa	ASE	Kappa Z-test (between the first case and others)
Bi-temporal data	87.3%	0.86	0.0216	N/A
Bi-temporal data plus 1-pixel radius NCIs	92.3%	0.91	0.0175	Significant (1.99)
Bi-temporal data plus 2-pixel radius NCIs	93.3%	0.92	0.0164	Significant (2.47)
Bi-temporal data plus 3-pixel radius NCIs	94.3%	0.94	0.0152	Significant (2.97)
Bi-temporal data plus 4-pixel radius NCIs	93.3%	0.92	0.0164	Significant (2.47)
Bi-temporal data plus 5-pixel radius NCIs	92.7%	0.92	0.0171	Significant (2.16)

b) Binary change classification results using a decision tree classifier.

Category	Number of rules	Overall accuracy	Kappa	Kappa Z-test (between the first case and others)
Bi-temporal data	10	90.7%	0.81	N/A
Bi-temporal data plus 1-pixel radius NCIs	4	98%	0.96	Significant (1.99)
Bi-temporal data plus 2-pixel radius NCIs	3	98.3%	0.96	Significant (2.47)
Bi-temporal data plus 3-pixel radius NCIs	5	99%	0.98	Significant (2.97)
Bi-temporal data plus 4-pixel radius NCIs	4	98.3%	0.96	Significant (2.47)
Bi-temporal data plus 5-pixel radius NCIs	6	97.7%	0.95	Significant (2.16)

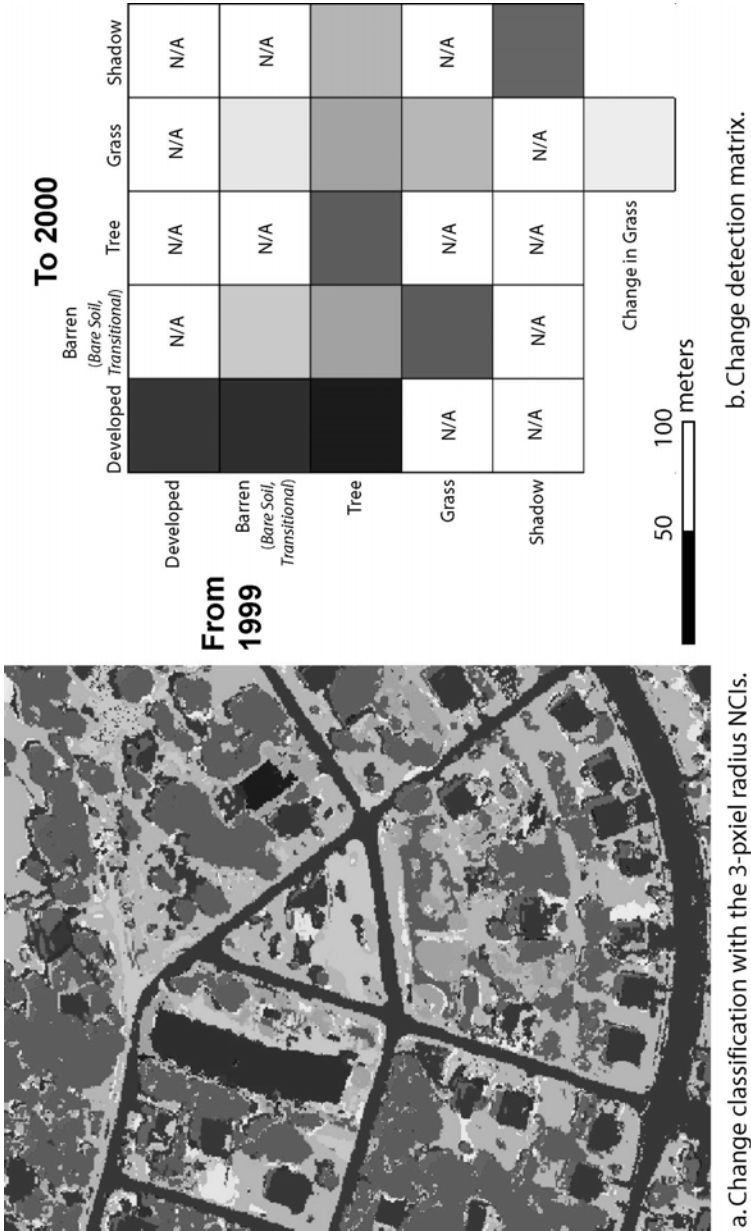


Fig. 6. a) Change classification output including the 3-pixel radius NCIs. b) Change detection matrix between two dates.

Three hundred samples were not sufficient to evaluate the change classification with the thirteen classes. For more reliable evaluation statistics, binary change detection was also conducted using the same reference data and decision tree classification. The decision tree binary classifications with the NCIs resulted in higher accuracies compared to the binary change detection without the NCIs (Table 1b). In addition, the number of rules generated from the decision trees was generally less than one-half of the number of rules from the decision tree without the NCIs. Binary change detection using the NCIs (i.e., without bi-temporal imagery) yielded very high accuracies over 97%.

These results support the use of neighborhood correlation image variables for change detection. Various levels of neighborhood correlation images have their own characteristics. The concept of neighborhood correlation images can be extended to “objects,” and object correlation images (OCIs) may be incorporated into object-oriented change detection.

2.4 Case Study 2 – Subsidence Detection Using Single-date LIDAR-derived Elevation Data

Human beings have produced large amounts of hazardous waste. Hazardous waste must be stored in safe places to avoid contaminating the environment. Monitoring hazardous waste sites is also an essential safety measure. One of the possible failures on hazardous waste sites is subsidence of surface materials such as claycaps due to damage to the storage underneath. The purpose of this study was to investigate the potential of single-date LIDAR data with dense postings to detect subsidence in experimental waste sites at the Savannah River National Laboratory (SRNL) near Aiken, SC.

SRNL installed claycaps to hold nuclear-related hazardous waste products buried in shallow pits (Jensen et al. 2006). Claycap monitoring is normally conducted through *in-situ* visual inspection, which is very costly and may miss early claycap failure. Conversely, it is possible to use remote sensing techniques such as photogrammetry or lidargrammetry to identify subsidence or other direct topographic expressions of claycap failure on the order of just a few centimeters (Garcia-Quijano 2006).

This project used LIDAR data obtained by an Optech ALTM 2050 sensor mounted on a Cessna 337 aircraft flown by Sanborn, Inc. of Charlotte, NC.

The LIDAR data were collected over SRNL on November 14, 2004. The LIDAR data collection included small footprint first and last return location (x , y , and z) and intensity data using a 1064 nm laser at a pulse repetition frequency (PRF) of 50 kHz. The nominal post spacing was 0.4 m at an altitude of 700 m above ground level (AGL) over an area of 2.6 km². Last return LIDR data were processed using TerraModel's TerraScan morphological filtering software, eliminating obstructions on the ground such as trees and buildings to generate a bare-Earth elevation. An accuracy assessment of the LIDAR-derived elevation is found in Garcia-Quijano et al. (2006). The elevation and hillshaded surfaces of the first returns and bare Earth LIDAR data using the IDW interpolation method are shown Figure 7. The experimental waste sites, which were used for subsidence investigation, are located in the middle-left of the surfaces. Figure 8 depicts the LIDAR-derived digital terrain model overlaid with 25 cm contours showing two locations of potential subsidence.



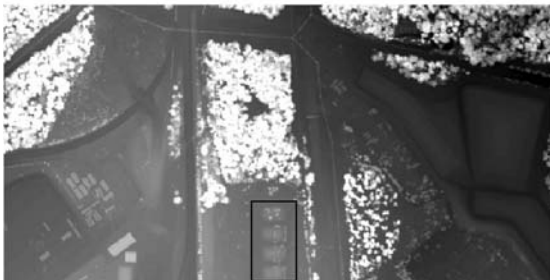
d. Hillshaded surface of the bare Earth elevation.



c. Elevation surface of the bare Earth using the IDW interpolation method.



b. Hillshaded surface of the first returns elevation.



a. Elevation surface of the first returns using the IDW interpolation method.

Fig. 7. Elevation surfaces of the first returns and bare-Earth LIDAR data using the IDW interpolation method (a and c) and the hillshaded surfaces of the elevation data (b and d).

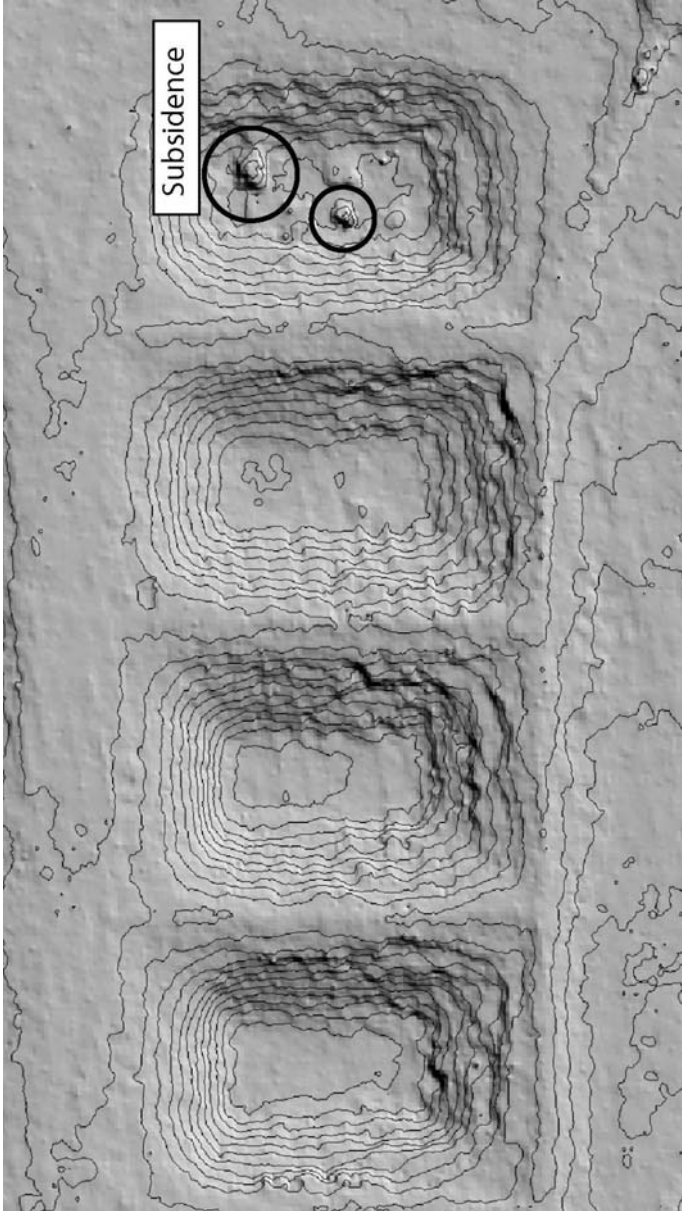


Fig. 8. LIDAR-derived digital terrain model with 25 cm contours showing two locations of potential subsidence.

The processing flow diagram of the study focusing on single date elevation-based subsidence analysis is summarized in Figure 9. The tabular LIDAR bare Earth data were imported into ESRI ArcMap 9.1 as a point shapefile. An elevation surface was generated based on the LIDAR bare Earth masspoints using an Inverse Distance Weighted (IDW) interpolation method (Figure 7). The elevation surface was used as reference elevation in the single elevation-based subsidence detection module. The logic of the single elevation-based subsidence detection include extraction of regular samples using the user-defined parameters, generation of simulated elevation surface using the regular samples and the IDW interpolation method, and creation of subsidence images from the difference between the reference and simulated elevation surfaces with a user-specified subsidence threshold.

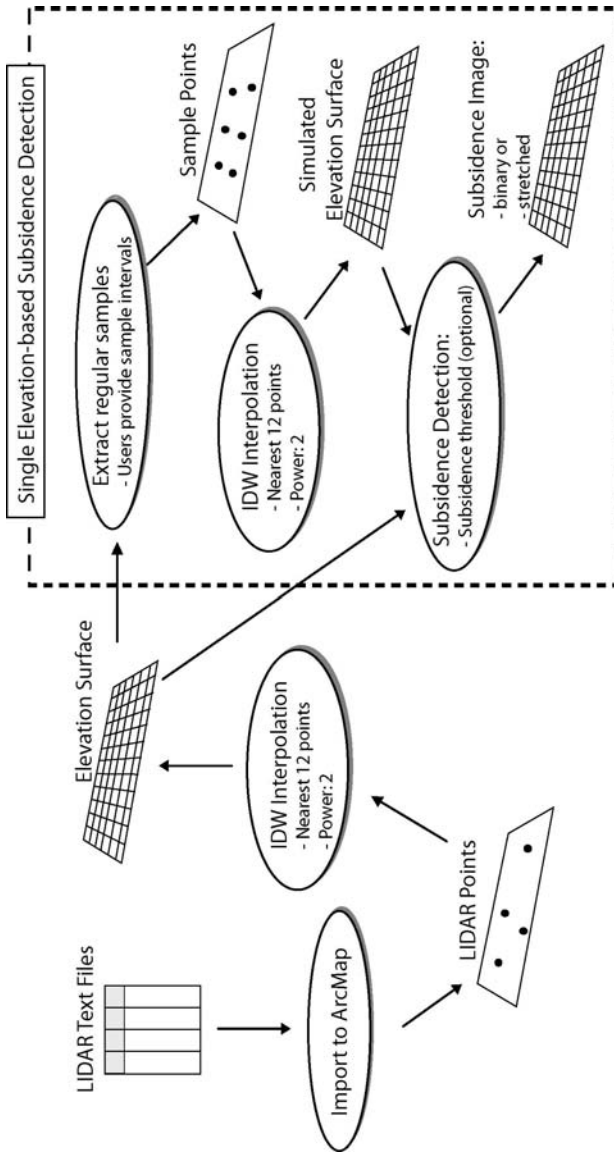


Fig. 9. Data processing flow diagram of single LIDAR-derived elevation-based subsidence detection.

Various user-specified parameters were applied to the single elevation-based subsidence detection module. The four selected subsidence detection results are shown in Figure 10. The subsidence detection based on the 3 m-interval sampling and 0.4 m threshold parameters yielded the best result (two locations inside the circle in Figure 10b). Although other combinations of parameters also detected the subsidence, most of them tended to overestimate subsidence, which resulted in false alarms on the normal claycaps. Those false alarms can be easily found in Figures 10c and 10d.

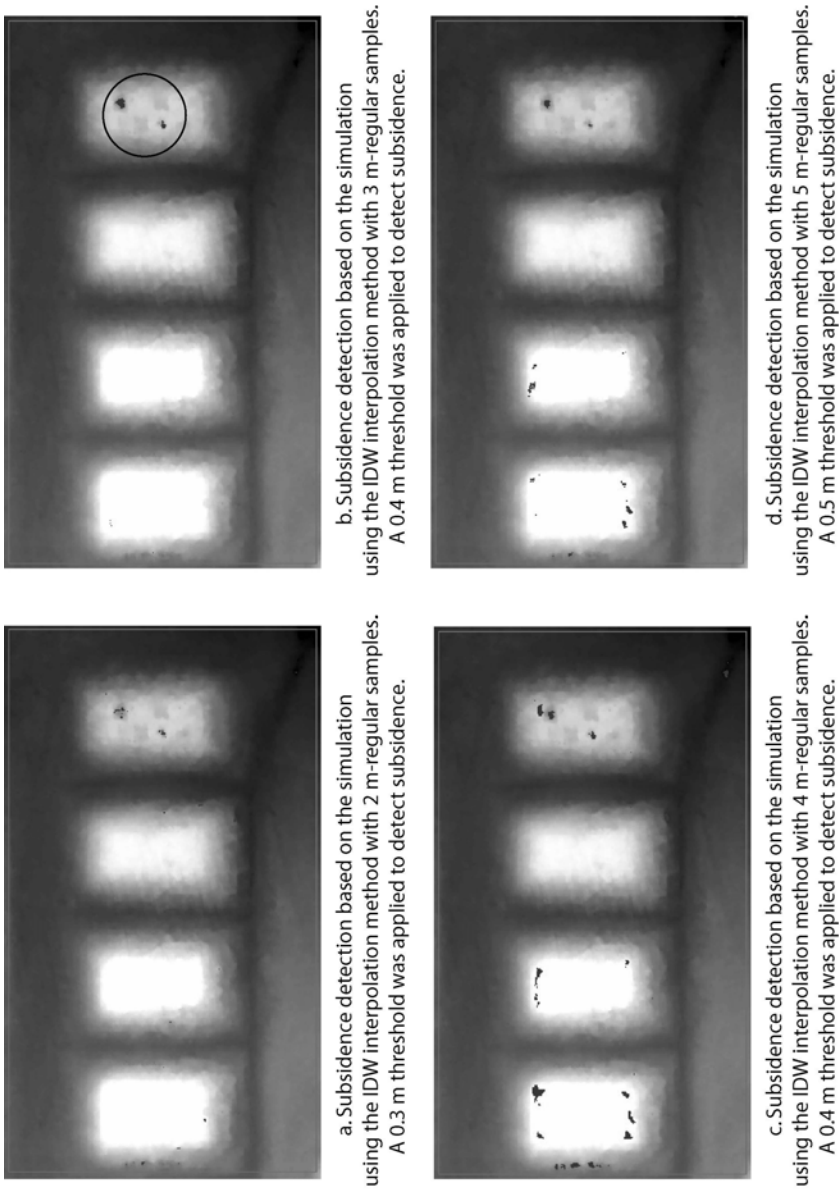


Fig. 10. Subsidence detection results associated with the experimental waste sites and using different parameters. The 3 m-interval sampling and 0.4 m threshold for subsidence resulted in the best result based on visual inspection.

Subsidence detection using multiple date (LIDAR-derived) elevation data may provide much more accurate and precise subsidence information. However, obtaining multiple date elevation data with high quality is not always possible. This study suggests that single-date quality elevation-based subsidence analysis can be an alternative to the multiple date approach in hazardous waste site monitoring.

2.5 Conclusion

As advanced remote sensors provide improved high-quality data, new and/or more sophisticated techniques are needed to extract accurate and reliable change information from the data. This chapter provided examples of the application of new digital change detection techniques using two different remote sensing data sources for change detection in urban environments.

References

- Baltsavias EP (1999) Airborne Laser Scanning: Basic Relations and Formulas. *ISPRS Journal of Photogrammetry & Remote Sensing* 54:199-214
- Boland J, 16 co-authors (2004) Chapter 8: Cameras and Sensing Systems. In McGlone JC (Ed.) *Manual of Photogrammetry* 5th Ed. Bethesda: ASP&RS 629-636
- Chan JC, Chan K, Yeh AG (2001) Detecting the Nature of Change in an Urban Environment: a Comparison of Machine Learning Algorithms. *Photogrammetric Engineering & Remote Sensing* 67(2):213-225
- Collins JB, Woodcock CE (1996) An Assessment of Several Linear Change Detection Techniques for Mapping Forest Mortality Using Multitemporal Landsat TM Data. *Remote Sensing of Environment* 56:66-77
- Coppin PR, Bauer ME (1996) Digital Change Detection in Forest Ecosystems with Remote Sensing Imagery. *Remote Sensing Reviews* 13:207-234
- Flood M, Gutelius B (1997) Commercial Implications of Topographic Terrain Mapping Using Scanning Airborne Laser Radar. *Photogrammetric Engineering & Remote Sensing* 63:327
- Garcia-Quijano M (2006) *Claycap Anomaly Detection using Hyperspectral Remote Sensing and Lidargrammetric Techniques*. Ph.D. Dissertation, Department of Geography, University of South Carolina, 141 p.
- Garcia-Quijano M, Jensen JR, Hodgson ME, Hadley BC, Gladden JB, Lapine LA (2006) Significance of Altitude and Posting-density on Lidar-derived Eleva-

- tion Accuracy on Hazardous Waste Sites. *Photogrammetric Engineering & Remote Sensing* in press.
- Im J, Jensen JR (2005). A Change Detection Model Based on Neighborhood Correlation Image Analysis and Decision Tree Classification. *Remote Sensing of Environment* 99:326-340
- Jensen JR (2005) *Introductory Digital Image Processing*. 3rd Ed. Upper Saddle River NJ: Prentice Hall 526 p.
- Jensen JR (2006) *Remote Sensing of the Environment: An Earth Resource Perspective*. 2nd Ed. Upper Saddle River NJ: Prentice Hall 592 p.
- Jensen JR, Garcia-Quijano M, Im J, Hadley BC, Gladden JB (2006) Development of a Remote Sensing and GIS-assisted Spatial Decision Support System for Hazardous Waste Site Monitoring. *Photogrammetric Engineering & Remote Sensing* in review
- Jensen JR, Rutchey K, Koch M, Narumalani S (1995) Inland Wetland Change Detection in the Everglades Water Conservation Area 2A Using a Time Series of Normalized Remotely Sensed Data. *Photogrammetric Engineering & Remote Sensing* 61(2):199-209
- Lu D, Mausel P, Brondizio E, Moran E (2004) Change Detection Techniques. *International Journal of Remote Sensing* 25(12):2365-2407
- Leonard J (2005) *Technical Approach for LIDAR Acquisition and Processing*. Frederick MD: EarthData Inc. 20 p.
- Maune DF (Ed.) (2001) *Digital Elevation Model Technologies and Applications: The DEM Users Manual*. Bethesda: ASP&RS 1151 p.
- Mikhail EM, Bethel JS, McGlone JC (2001) *Introduction to Modern Photogrammetry*. NY: John Wiley 479 p.
- Quinlan JR (2003) *Data Mining Tools See5 and C5.0*. St. Ives NSW Australia: RuleQuest Research <http://www.rulequest.com/see5-info.html>